AIP | Advances

An unshielded radio-frequency atomic magnetometer with sub-femtoTesla sensitivity

David A. Keder, David W. Prescott, Adam W. Conovaloff, and Karen L. Sauer

Citation: AIP Advances **4**, 127159 (2014); doi: 10.1063/1.4905449
View online: http://dx.doi.org/10.1063/1.4905449
View Table of Contents: http://scitation.aip.org/content/aip/journal/adva/4/12?ver=pdfcov
Published by the AIP Publishing

An unshielded radio-frequency atomic magnetometer with sub-femtoTesla sensitivity

David A. Keder, David W. Prescott, Adam W. Conovaloff,
and Karen L. Sauer[a]
School of Physics, Astronomy, and Computational Sciences, George Mason University, Fairfax, Virginia, 22030, USA

(Received 3 October 2014; accepted 19 December 2014; published online 31 December 2014)

We demonstrate a radio-frequency potassium-vapor magnetometer operating with sensitivities of 0.3 fT/$\sqrt{\text{Hz}}$ at 0.5 MHz and 0.9 fT/$\sqrt{\text{Hz}}$ at 1.31 MHz in the absence of radio-frequency and mu-metal or magnetic shielding. The use of spatially separated magnetometers, two voxels within the same cell, permits for the subtraction of common mode noise and the retention of a gradient signal, as from a local source. At 0.5 MHz the common mode noise was white and measured to be 3.4 fT/$\sqrt{\text{Hz}}$; upon subtraction the noise returned to the values observed when the magnetometer was shielded. At 1.31 MHz, the common mode noise was from a nearby radio station and was reduced by a factor of 33 upon subtraction, limited only by the radio signal picked up by receiver electronics. Potential applications include in-the-field low-field magnetic resonance, such as the use of nuclear quadrupole resonance for the detection of explosives.
[http://dx.doi.org/10.1063/1.4905449]

Alkali metal vapor based optical magnetometers have gained popularity within the last decade as a candidate technology for applications requiring ultra-sensitive detection of magnetic fields.[1] Their remarkable sensitivities, rivaling those of superconducting quantum interference device (SQUIDS),[2–5] without requiring cryogenics have motivated research for use in practical applications where precise magnetic field sensing at frequencies from as low as 10 Hz to the radio-frequency (RF) regime is required. These optical atomic magnetometers have shown promise in NMR spectroscopy,[6,7] MRI,[8,9] and medical applications such as encephalography and cardiography;[10–12] there is also potential for miniaturization to chip-scale sizes for integration in hand-held devices.[13] In addition to the advantages of sensitivity, atomic magnetometers are unperturbed by electric fields oscillating at RF frequencies, as opposed to detection through wire loops, either as used for SQUID or conventional Faraday coils. Furthermore, the atomic sensors are not susceptible to the inductive coupling that complicates the use of coil arrays for RF interference mitigation. These advantages make atomic magnetometers especially good candidates for interference mitigation at RF frequencies.

Most experimental work to date in the RF range has been done enclosed within passive metal shielding[14–17] protecting the magnetometer from ambient static magnetic fields as well as RF noise and interference, an impractical configuration for field applications, for example the detection of contraband substances by nuclear quadrupole resonance (NQR).[17–19] We demonstrate the operation of a two-channel unshielded RF atomic magnetometer serving as a gradiometer, sensitive to local signals while rejecting noise and interference from distant RF sources. Sub-fT/$\sqrt{\text{Hz}}$ sensitivity is obtained with an unshielded atomic magnetometer, more than order of magnitude improvement over previous results at any frequency.[6,7,11] The operation is in principle similar to multi-channel magnetometers operating at much lower frequencies, <200 Hz,.[20–22] These magnetometers,[20–22] however, operate close to zero field and have as a primary target application biological magnetic fields, which vary

[a]Electronic mail: ksauer1@gmu.edu

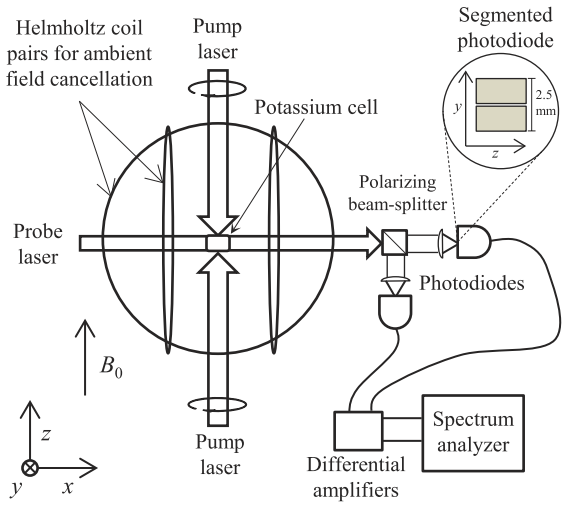

FIG. 1. Experimental setup of the unshielded magnetometer. A heated glass cell containing potassium is optically pumped using circularly polarized beams from a diode laser tuned to the D1 line. The linearly polarized probe beam tuned off-resonance is sent through the cell to a balanced polarimeter containing a pair of photodiodes. Each photodiode is segmented in order to be able to separate signals coming from the top part of the cell, in the y-direction, from the bottom. In addition to the Helmholtz pairs shown above, a set of coils (not shown) closer to the cell creates the tuning magnetic field $B_0\hat{z}$ and corrects for first order gradients ∂B_z. RF coils, also not shown, near the cell provide uniform and gradient test signals.

relatively slowly in time, $f < 100$ Hz. In contrast, the magnetometer described here is tuned using a static magnetic field to get to the three-four orders of magnitude higher resonance frequencies required for RF spectroscopy. Rejection of interference, such as from radio stations, relies heavily on the matching of Larmor frequencies in the channels, thus putting strict requirements on the homogeneity of the larger magnetic fields required for RF detection.

Figure 1 shows the experimental setup, which is similar to those of Refs. 17 and 23. A $4 \times 4 \times 6$ cm borosilicate glass cell containing a droplet of 99.95% pure potassium, 650 torr of He as a buffer gas, and 50 torr of N_2 as a quenching gas is heated to 175 °C via forced hot air within a nonmetallic oven with four windows for optical access. The K vapor is optically pumped from two directions simultaneously to the $|F = 2; m_F = 2\rangle$ Zeeman state by a circularly polarized single-mode diode laser tuned to the D1 line of potassium. A linearly polarized beam from an additional laser, blue-detuned from the D1 line by 0.11 nm, is sent through the cell orthogonal to the pump beam. The probe power was about 75 mW, while total pump power was 350 mW. The longitudinal polarization attained, $\langle F_z \rangle/2$, was close to 100%.

Both beams were passed through a Keplerian expansion scheme to uniformly fill the cell. Any transverse magnetization of the potassium vapor in $\hat{x}$ is projected onto the polarization of the probe beam via Faraday rotation. The angle of polarization of the probe beam is read by a balanced polarimeter, consisting of two bi-segmented photodiodes, placed so that portions of the beam probing the upper and bottom halves of the cell are projected onto different photodiode elements, effectively splitting the cell into two voxels separated by 2 cm in the y-direction. Achromatic doublets are used in the polarimeter to correct for imaging abberation. The top and bottom of the cell are defined by an anti-Helmholtz pair of rectangular coils placed symmetrically around the cell and mounted directly on the oven; the field direction of interest B_y, as opposed to B_x, is identified by the phase of the signal. A phase-sensitive spectrum analyzer is used to analyze the signal from the photodiode.

Compensation for ambient static magnetic fields in $\hat{x}$ and $\hat{y}$ is accomplished with pairs of circular coils in a Helmholtz configuration. The tuning magnetic field in $\hat{z}$ is produced by four coil sets wound on a 20 cm diameter cylindrical form. One set produces the static field in $\hat{z}$, and the remaining coil sets correct for linear gradients in B_z. Inhomogeneities in the tuning field across the volume of the cell will serve to broaden the magnetometer's measurement linewidth, reducing the signal size and compromising the sensor's sensitivity. The coil currents are chosen to maximize the magnetometer's response

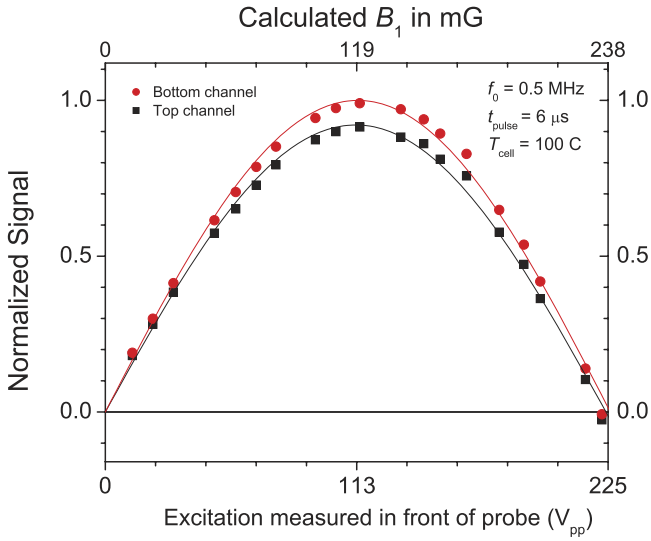

FIG. 2. Color online. For the top (black squares) and bottom (red circles) channels, calibration of the 0.5 MHz field was done using 6 μs pulses of varying strength. A similar calibration was done for 1.3103 MHz.

to a uniform test signal produced at the frequency of interest and to match the Larmor frequencies of both halves of the cell.

To ensure optimal subtraction of common-mode noise and interference, calibration of the two data channels with respect to each other is necessary to account for differences in signal-response caused by the static magnetic field and laser power intensity variations between the voxels. A uniform test signal is generated by a RF coil across the cell. The phase sensitive detection of the spectrum analyzer gives a complex signal, the real portion corresponding to a component in phase with the RF generator and the imaginary to an out-of-phase component. The steady-state response of the magnetometer to the driven signal is measured in the two channels, and the ratio of the complex peaks at the driving frequency serves as a simple transfer function to standardize the channels. The strength of the test signal is calibrated against the field used for an electron spin-resonance experiment in which the net polarization is fully tipped in the transverse plane by a strong short pulse. This calibration, an example of which is shown in Fig. 2, is done at relatively low temperature, 100 C, to keep the net Faraday rotation $\theta_F < \pi/4$ so as to avoid the non-linearities associated with larger rotations.[24] At the frequencies of interest, the Zeeman resonances are only partially resolved, creating complicated spectra, and so we use the initial amplitude of the free induction decay as the signal in this calibration. We adopted this calibration after determining that a DC calibration of the RF coil was not representative of the correct calibration at the RF frequencies due to increased inductive and capacitive coupling of the field coils.

Measurements were taken at two frequencies. The first frequency, 0.5 MHz, was chosen for its proximity to NQR frequencies of interest for substance detection.[17] The second frequency, 1.3103 MHz, was chosen for its proximity to a known source of distant interference, radio station 1310 AM WDCT. After channel calibration, measurements were taken with a linear RF gradient field, $\partial B_y/\partial y$, produced by the anti-Helmholtz pair and at the calibration frequency to simulate a local source. To characterize environmental and instrumental noise, measurements were also taken with the resonant magnetic field detuned from the calibration frequency and the pump or probe light blocked. Results at both frequencies are shown in Fig. 3, with data channels added (normal mode) or subtracted (gradiometer mode). Only the real portion of the signal is shown in the figure.

Expected values for ambient magnetic noise at our frequencies of interest are given in Ref. 25. At $f = 0.5$ MHz in an urban environment, magnetic noise from man-made sources is the dominant type of noise, with median ambient noise of roughly 1 fT/$\sqrt{\text{Hz}}$; variations in this number with time of day and specific location are on the order of ± 10 dB. Data from more recent studies however suggest that for indoor environments, values of magnetic noise could exceed this figure by 20 dB,[26]

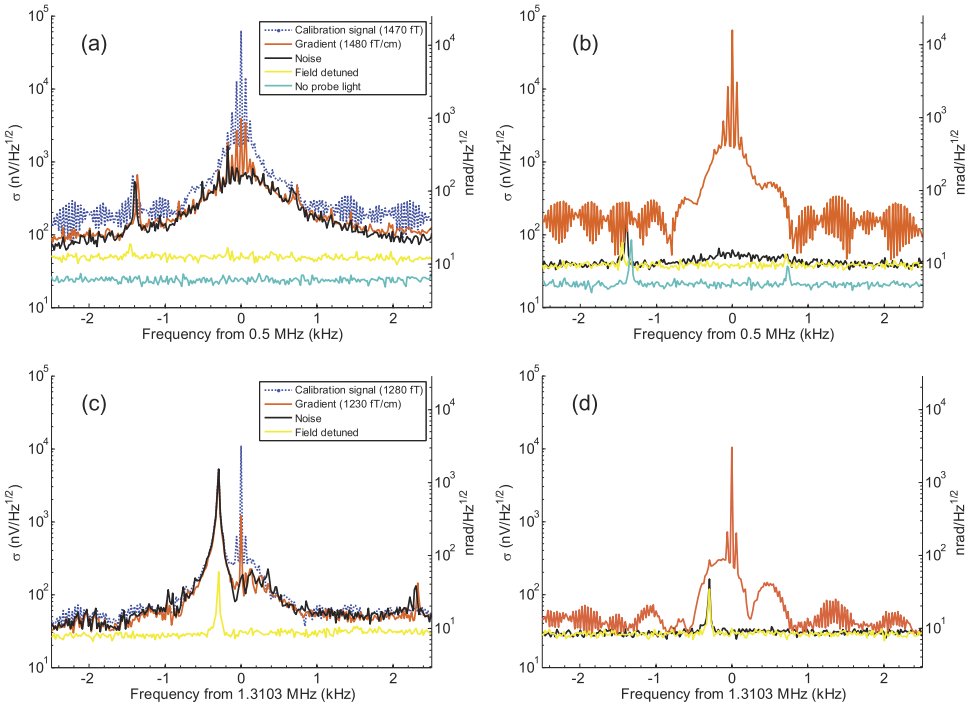

FIG. 3. Color online. The ambient room noise (black) is 3.4 fT/$\sqrt{\text{Hz}}$ at 0.5 MHz as shown by adding the magnetometer channels (a). By subtracting the channels (b) this noise is reduced to 0.33 fT/$\sqrt{\text{Hz}}$ and the gradient signal (orange) is clearly revealed. (c) A 600 fT_{rms} interference signal from a nearby radio-station is observed close to 1.31 MHz when the channels are added. Upon subtraction (d) the radio-signal is reduced by a factor of 33 or down to the level of the interference in the electronics, as can be seen by comparison to the noise when the resonant field is detuned from 1.31 MHz (yellow); further a 0.9 fT/$\sqrt{\text{Hz}}$ sensitivity is regained and the gradient signal becomes apparent. The structure observed in the calibration (dotted blue) and gradient signals is due to windowing effects and additional noise arising from RF generator itself. The y-axes represent standard deviation around zero and the frequency resolution is 20 Hz on the x-axis.

though the available amount of data at this frequency is limited. At 0.5 MHz with channels added, we observe ambient magnetic noise values of 3.4 fT/$\sqrt{\text{Hz}}$, supporting the higher noise expected for indoor operation, and roughly consistent with the $f^{-0.4}$ dependence inferred from Ref. 25 and 13 fT/$\sqrt{\text{Hz}}$ measured by Ref. 6 at 75 kHz with an unshielded RF atomic magnetometer. Radio signals and other sources of coherent man-made interference do not, however, follow such an inverse frequency law and so we addressed this experimental condition separately.

With channels subtracted, the effects of common noise across the magnetometer cell are reduced by an order of magnitude, down to 0.33 fT/$\sqrt{\text{Hz}}$. At 0.5 MHz, the magnetometer sensitivity appears to be limited by magnetic noise generated by nearby sources or potentially light-shift noise.[15] Measurements taken with the resonant field detuned from 0.5 MHz show the lower contribution to the noise from the probe beam and electronics. Further, blocking the probe beam allowed for the measurement of baseline electronic noise from the instrumentation, which is lower than the probe laser noise. Noise levels observed with only the pump light blocked (not shown) are equivalent to those obtained with the resonant field detuned at both frequencies of interest. This implies that spin-projection noise, which would be observable in the absence of pump light,[27] does not limit the magnetometer.

At 1.310 MHz, we experienced interference and noise not only at the radio station's carrier frequency (1.31 MHz), but from broadcast sidebands which extend out ±5 kHz. With channels added, we were able to detect a magnetic signal from the broadcast of 600 fT_{rms}. Reradiation of the AM radio broadcast by the DC magnetic field coils severely undermined interference rejection in gradiometer mode. To mitigate reradiation, the two strands feeding each DC field coil were wound through a series of four ferrite toroids; three wound for differential mode and one for common mode rejection. Further metallic braid was used to sheath these filtered cables. Under these conditions we were able to obtain high interference rejection. A sensitivity of 0.9 fT/$\sqrt{\text{Hz}}$ was calculated from the 1280 fT calibration

signal. This degradation in sensitivity, compared to that at 0.5 MHz, is mainly attributed to the larger field gradients of the tuning magnetic field across the magnetometer cell for the higher Larmor frequency; T_2 values dropped from 0.53 and 0.48 ms at 0.5 MHz to 0.16 and 0.15 ms at 1.31 MHz for the top and bottom voxels. The subtracted data was limited by shot noise from the probe beam. The interference peak at 1.31 MHz was reduced to the baseline levels of the experimental instrumentation; a rejection ratio of 33:1 of the radio station's carrier frequency was obtained. The radio station is approximately 3 km from the laboratory and so, given the distance between the channels, one can estimate a potential rejection ratio of 10^5 from far-field radiation, underscoring that electrical pick-up by instrumentation prevented a higher rejection ratio. Better cabling design and shielding on the balanced polarimeter electronics and receiver would further reduce this pick-up. To get a sense of the potential reduction, we took as the transfer function the average complex ratio between the channels when the radio-station dominated the spectrum. In this case the rejection ratio becomes 132:1, bringing the interference signal down close to the background noise level.

The sub-femtoTesla sensitivities and high interference rejection attained with a two-voxel RF atomic magnetometer in an unshielded environment demonstrate the potential of these types of sensors for sensitive detection of weak RF fields from local sources with strong RF interference mitigation, such as the in-situ detection of explosives or other contraband materials with low-field magnetic resonance techniques. While this work was done with a relatively large cell, ~100 cm^3, recent development of very compact, ~1 cm^3, magnetometers, which use multiple passes of the probe beam and obtain sub-femtoTesla sensitivity,[24] will permit more versatile interference rejection schemes.

ACKNOWLEDGEMENTS

We gratefully acknowledge helpful discussions with Mark Monti and Jeffrey Okamitsu of NIITEK, Inc. about RF interference mitigation, and with Michael Romalis of Princeton University in review of this manuscript. This work was supported by NIITEK Inc., DARPA Contract No. HR0011-13-C-0058, and NSF Grant No. 0730473. A.C. would like to acknowledge support from George Mason University's Presidential Fellowship and D.K. would like to acknowledge support from the Undergraduate Research Scholars Program at Mason.

[1] D. Budker and M. Romalis, Nat. Phys. **3**, 227 (2007).
[2] M. Simmonds, W. Fertig, and R. Giffard, Magnetics, IEEE Transactions on **15**, 478 (1979).
[3] D. M. TonThat and J. Clarke, Review of Scientific Instruments **67** (1996).
[4] H. Seton, J. Hutchison, and D. M. Bussell, Applied Superconductivity, IEEE Transactions on **7**, 3213 (1997).
[5] D. F. He, M. Tachiki, and H. Itozaki, Superconductor Science and Technology **21**, 015023 (2008).
[6] I. M. Savukov, S. J. Seltzer, and M. V. Romalis, Journal of Magnetic Resonance **185**, 214 (2007).
[7] G. Bevilacqua, V. Biancalana, Y. Dancheva, and L. Moi, Journal of Magnetic Resonance **201**, 222 (2009).
[8] S. Xu, V. V. Yashchuk, M. H. Donaldson, S. M. Rochester, D. Budker, and A. Pines, Proceedings of the National Academy of Sciences **103**, 12668 (2006).
[9] I. Savukov and T. Karaulanov, Applied Physics Letters **103**, 043703 (2013).
[10] H. Xia, A. Ben-Amar Baranga, D. Hoffman, and M. V. Romalis, Applied Physics Letters **89**, 211104 (2006).
[11] J. Belfi, G. Bevilacqua, V. Biancalana, S. Cartaleva, Y. Dancheva, and L. Moi, J. Opt. Soc. Am. B **24**, 2357 (2007).
[12] K. Kim, S. Begus, H. Xia, S.-K. Lee, V. Jazbinsek, Z. Trontelj, and M. V. Romalis, NeuroImage **89**, 143 (2014).
[13] P. D. D. Schwindt, S. Knappe, V. Shah, L. Hollberg, J. Kitching, L.-A. Liew, and J. Moreland, Applied Physics Letters **85**, 6409 (2004).
[14] W. Chalupczak, R. M. Godun, S. Pustelny, and W. Gawlik, Applied Physics Letters **100**, 242401 (2012).
[15] I. M. Savukov, S. J. Seltzer, M. V. Romalis, and K. L. Sauer, Phys. Rev. Lett. **95**, 063004 (2005).
[16] I. M. Savukov, V. S. Zotev, P. L. Volegov, M. A. Espy, A. N. Matlashov, J. J. Gomez, and R. Kraus, Jr., Journal of Magnetic Resonance **199**, 188 (2009).
[17] S.-K. Lee, K. L. Sauer, S. J. Seltzer, O. Alem, and M. V. Romalis, Applied Physics Letters **89**, 214106 (2006).
[18] A. Garroway, M. Buess, J. Miller, B. H. Suits, A. Hibbs, G. Barrall, R. Matthews, and L. Burnett, Geoscience and Remote Sensing, IEEE Transactions on **39**, 1108 (2001).
[19] J. B. Miller and G. A. Barrall, American Scientist **93**, pp. 50 (2005).
[20] C. Affolderbach, M. Stähler, S. Knappe, and R. Wynands, Applied Physics B **75**, 605 (2002).
[21] I. K. Kominis, T. W. Kornack, J. C. Allred, and M. V. Romalis, Nature **422**, 596 (2003).
[22] S. J. Seltzer and M. V. Romalis, Applied Physics Letters **85** (2004).
[23] O. Alem, K. L. Sauer, and M. V. Romalis, Phys. Rev. A **87**, 013413 (2013).
[24] D. Sheng, S. Li, N. Dural, and M. V. Romalis, Phys. Rev. Lett. **110**, 160802 (2013).
[25] *Recommendation ITU-R PI.372-11 - Radio Noise* (Radiocommunication Sector of International Telecommunication Union, Geneva, 2013).
[26] F. Leferink, F. Silva, J. Catrysse, S. Batterman, V. Beauvois, and A. Roc'h, Radio Science Bulletin 49 (2010).
[27] V. Shah, G. Vasilakis, and M. V. Romalis, Phys. Rev. Lett. **104**, 013601 (2010).